Original Article

DOI: 10.5582/bst.2025.01316

Hearing impairment in Parkinson's disease models: Possible relation with changes in cochlear efferent fibers

Hao Zhao[1,§], Shijun Peng[2,§], Rui Zhao[1], Tongxiang Diao[1], Yixin Zhao[1], Xin Ma[1], Hongwei Zheng[1,*], Yixu Wang[1,*], Lisheng Yu[1,*]

[1] Department of Otolaryngology, Head and Neck Surgery, Peking University People's Hospital, Beijing, China;
[2] Department of Neurosurgery, People's Hospital, Peking University, Beijing, China.

SUMMARY: Hearing impairments, as a prevalent and debilitating non-motor symptom of Parkinson's disease (PD), remain unclear in mechanisms. In this work, we established PD mouse and rat models by using 1-Methyl-4-phenyl-1,2,3,6-tetrahydropyridine (MPTP) and 6-hydroxydopamine (6-OHDA), respectively, and investigated their hearing functions and potential mechanisms through auditory brainstem response (ABR), distortion product otoacoustic Emissions (DPOAE), noise exposure, immunofluorescence labeling, volumetric measurement, and colocalization analysis. In MPTP-induced PD mice, we observed significant cholinergic fibers decompensation, heterogeneous dopaminergic fibers damage of cochlear efferent fibers, and adrenergic sympathetic fibers marked loss in the osseous spiral lamina (OSL), corresponding to insignificant cochlear hair cells, ribbon synapse alteration, and auditory sensitivity injury. While in 6-OHDA-induced PD rats, asymmetric alterations in cochlear cholinergic, dopaminergic fibers were found, accompanied by inconsistent adrenergic changes in the OSL, which matched unilateral hair cells, ribbon synapse damage, and hearing loss. Overall, findings from this work indicate that pathological alterations in the cochlea of PD mice and rats, particularly in efferent fibers, may be closely relevant to peripheral hearing alterations.

Keywords: Parkinson's disease, hearing loss, cholinergic fibers, dopaminergic fibers, sympathetic fibers

1. Introduction

Parkinson's disease (PD), the second most common progressive neurodegenerative disorder, is a major contributor to rising global disability rates. In recent years, PD-related prevalence, disability rates, and mortality have shown an upward trend (*1*). The etiology of PD remains unknown. It is characterized primarily by early dopaminergic neuronal loss in the substantia nigra of the basal ganglia, accompanied by classic Parkinson's disease manifestations and secondary motor symptoms. Furthermore, non-motor symptoms that usually precede typical PD manifestations have garnered significant attention, which include fatigue, gastrointestinal disturbances, and sensory deficits (visual impairment, olfactory dysfunction, and hearing impairment). Compared with studies on olfactory dysfunction and visual impairment, previous research on hearing impairment has been relatively insufficient (*2*). Population-based case-control studies indicate a 1.6% association between clinical hearing impairment and PD (*3,4*). Interestingly, studies have found that, similar to motor symptoms, auditory symptoms in PD patients also exhibit lateralization — meaning more pronounced hearing loss occurs on the side with more severe PD symptoms (*5*). However, the mechanisms underlying hearing impairment in PD patients remain unclear. Recent research suggests its potential association with dysfunction of dopamine transporters in the basal ganglia (*6*).

Dopamine is primarily produced in the striatal structures of the substantia nigra and regulates processes such as movement, attention, reward, and motivation. Growing evidence indicates dopamine also participates in auditory processing, with fibers present in auditory structures including the auditory cortex, thalamus, superior olivary complex, and inferior colliculus. This involvement occurs primarily through dopamine receptors, notably dopamine receptor 2 (D2) (*7,8*). Recent studies have identified the subperiventricular nucleus (SPF) of the thalamic bundle as a potential key hub coordinating the balance of neurotransmitters — including glutamate and glycine — between various auditory structures such as the inferior colliculus and superior olivary complex (*7,9*). Dopaminergic fibers in the cochlea primarily originate from lateral olivocochlear

neurons (LOC), projecting onto afferent fibers adjacent to inner hair cells. These fibers inhibit excessive excitation of afferent neurons *via* nearby dopamine receptor 1 (D1) and D2 receptors, predominantly D2 receptors, acting in concert with cholinergic fibers — another component of LOC fibers — to coordinate function (*7,10,11*). However, the precise function of LOC remains unclear. The prevailing view suggests it possibly majors in adaptation to acoustic environments and balances subtle bilateral activity. In contrast, medial olivocochlear neurons (MOC) primarily project cholinergic fibers that synapse with the basal ends of outer hair cells. They mainly regulate excitability of bilateral outer hair cells, participating in auditory sensitivity modulation under varying sound backgrounds and spatial auditory discrimination (*10,12,13*).

Recent research on the auditory system in PD has primarily focused on regions such as the auditory cortex and basal ganglia, with greater emphasis on its role in auditory-related cognition and emotion (*10,14,15*). However, studies on peripheral hearing, particularly cochlear pathophysiological changes in PD models, remain scarce. Thus, this study mainly focuses on the hearing changes and cochlear pathological alterations, especially changes in olivocochlear efferent fibers, in PD mice and rat models, to provide new insights for investigating mechanisms and treatments for hearing loss in PD.

2. Materials and Methods

2.1. Animals and drug treatments

Due to the hearing-protective effects of estrogen and the high mortality rate of female mice in PD modeling, only male animals were used in this study (*16,17*). Male C57BL/6J mice (7 weeks old) and male Sprague-Dawley (SD) rats (10 weeks old) were purchased from the Animal Experiment Center of Peking University People's Hospital (PKUPH). This study was approved by the Institutional Animal Care and Use Committee (IACUC) at PKUPH (No. 2023PHE025). All animals were housed in a controlled, specific pathogen-free environment (temperature, 23 ± 3°C; humidity, 55% ± 15%; 12/12 h light/dark cycle) with free access to food and water. Following work based on previous studies, mice with abnormal hearing were excluded (*18-22*). The remaining mice were randomly assigned to two groups: the MPTP group (model group), which received intraperitoneal injections of MPTP-HCl (Sigma, St. Louis, MO, USA, M0896, 30 mg/kg) once daily for 5 days, while the control group received an equivalent volume of saline *via* intraperitoneal injection once daily for 5 days (*18-22*). Subsequent experiments were conducted according to the experimental protocol without a time interval. Mice in two groups underwent behavioral testing, open field test, and audiological assessment, ABR and DPOAE, followed by tissue collection for pathological examination of the brain and cochlea immediately. Based on the successful establishment of the PD model, confirmed by behavioral and pathological analyses, findings regarding audiology and cochlear morphology were obtained (Supplementary Figure S1 A, *https://www.biosciencetrends.com/action/getSupplementalData.php?ID=279*). SD rats were screened for hearing abnormalities and excluded as described previously (*23-26*). Rats underwent unilateral 6-OHDA lesions of the substantia nigra pars compacta (SNc). Briefly, rats anesthetized with sodium pentobarbital (40 mg/kg, ip) were fixed in a stereotaxic apparatus (SN-2 N, Narishige, Tokyo, Japan) and injected with 6-OHDA (2 μg/μL) into the right SNc (AP -5.2 mm, ML -2.0 mm, DV -8.0 mm). Fifteen minutes before 6-OHDA injection, rats received pretreatment with dexepamine (25 mg/kg, ip) to protect noradrenergic neurons. Control rats received an equivalent injection of physiological saline containing 0.02% ascorbic acid (*23-26*). Subsequent procedures were performed according to the experimental protocol after 3 weeks. Both groups of rats underwent behavioral testing, open field test, and audiological assessment, ABR and DPOAE, followed by tissue collection for pathological examination of the brain and cochlea immediately. Based on successful establishment of the PD model, confirmed by behavioral and pathological analyses, findings regarding audiology and cochlear morphology were obtained (Supplementary Figure S2 A, *https://www.biosciencetrends.com/action/getSupplementalData.php?ID=279*).

2.2. Open field test

Before testing, mice or rats were acclimated for 2 hours in their home cages within a quiet room. The open field arena (mice: 50 cm × 50 cm × 40 cm, white background; rats: 4 × 50 cm × 50 cm × 40 cm, white background) was placed in a soundproof chamber illuminated by indirect artificial light. The arena was thoroughly cleaned with a 5% ethanol/water solution between trials. One animal (mouse or rat) was positioned in the center of the arena, and spontaneous behavior was recorded for 10 minutes. Subsequently, video recordings were evaluated using the SMART video tracking system (Panlab, Barcelona, Spain).

2.3. Brain tissue immunofluorescence and immunohistochemistry

Mice or rats were deeply anesthetized and perfused with physiological saline, followed by injection of 4% polyformaldehyde (PFA) in 0.1 mol/L phosphate-buffered saline (water, PBS, pH 7.4). Brains were dissected and immersed in the same fixative for 12 hours, then dehydrated in 30% sucrose solution. Frozen brain tissue was sectioned into 30 μm-thick slices using a cryostat (Leica Biosystems, Nuremberg, Germany).

For immunofluorescence, sections were rinsed with PBS and blocked with a PBS solution containing 5% BSA and 0.5% Triton X-100 as antibody diluent. Sections were incubated with anti-tyrosine hydroxylase antibody (1:100, 58844, Cell Signaling Technology) at 4°C for 12 hours, washed three times with PBS, and subsequently incubated with secondary antibody for 2 hours. Finally, slides were sealed with anti-fade mounting medium containing DAPI (P0126, Beyotime, Shanghai, China) and imaged using a confocal microscope (Leica, Stellaris). For immunohistochemistry, sections were blocked with PBS containing 5% BSA, 1% normal goat serum, and 0.3% Triton X-100, then incubated overnight at 4°C with anti-tyrosine hydroxylase antibody (1:300, 58844, Cell Signaling Technology). Sections were incubated at room temperature for 2 h with biotinylated secondary antibody, followed by incubation for 1 h with ABC reagent (1:500, Vector Laboratories) and visualized using DAB substrate (Vector SK-4100). Slides were dehydrated through graded ethanol, cleared in xylene, and mounted with neutral resin coverslips. Brightfield images were captured using an Olympus BX53 microscope (Olympus).

2.4. ABR and DPOAE measurement

Before ABR testing, mice or rats were anesthetized *via* intraperitoneal (i.p.) injection of 0.7% sodium pentobarbital (25–50 mg/kg). For ABR recordings, three needle electrodes were placed subcutaneously: at the vertex, behind the test ear, and on the contralateral auricle. ABR thresholds were measured and recorded using a TDT system (RZ6 TDT; Tucker Davis Technologies hardware and SigGen/BioSig software; Alachua, Florida, USA) at a sampling rate of 21.1 Hz, delivered *via* a closed-field microphone system at various stimulus frequencies (4, 8, 16, 24, and 32 kHz). Sound stimuli began at 90 dB SPL and were decreased in 5 dB increments until ABR waves were no longer readily detectable. DPOAE measurements were conducted following ABR testing. The f1-f2 DPOAE was evaluated using TDT's real-time signal processing system II (RZ6 TDT; Tucker Davis Technologies hardware and SigGen/BioSig software). The DPOAE threshold is defined as the peak at 2f2-f1. During the testing process, a double-blind approach was adopted, and the sample size was determined based on biological replicates.

2.5. Noise exposure

Mice were placed in stainless steel cages positioned beneath a loudspeaker. Noise was generated by a loudspeaker (Aijie Audio Equipment Factory) driven by a power amplifier (MF-1201 MOSTET, ATech) and attenuator (PA5 TDT, Alachua, FL, USA). White noise at 108 dB sound pressure level (SPL) was used for 2 h to induce exposure. Calibration was measured using a sound level meter (Model 1200; Quest Technologies) before exposure. Ambient background noise around the cages was 45 dB. Control mice were placed in the same cages and the noise exposure chamber without noise activation for 2 h.

2.6. Immunofluorescence of the basilar membrane

Mice or rats were euthanized using carbon dioxide anesthesia, and bilateral cochleae were collected and fixed overnight in 4% paraformaldehyde at 4°C. The following day, cochleae were decalcified at room temperature using 10% EDTA for 5–6 hours (for mice) or 48–72 hours (for rats). After decalcification, the basilar membrane was carefully dissected and placed in PBS containing 0.3% Triton X-100 for 10 minutes; this process was repeated twice. Subsequently, the basilar membrane was blocked with 10% donkey serum for 2 hours, then incubated with the primary antibody overnight at 4°C. The following day, the basilar membrane was washed three times with PBS for 10 minutes each, and then incubated with the secondary antibody for 1 hour in the dark. Finally, the basilar membrane was stained with or without DAPI for 15 minutes. After washing as described above, the sample was mounted in medium and imaged using a confocal microscope (Leica, Stellaris).

Hair cells counting: The basilar membrane of the cochlea was divided into three turns, labeled with phalloidin (1:2000, A30104, ThermoFisher), and quantified under a 40× objective field.

Synaptic ribbon counting: Synaptic ribbons, associated with inner hair cells and myelinated afferent auditory nerves, were labeled with anti-C-terminal binding protein 2 (Ctbp2) (1:200, 612044, BD Biosciences), while hair cells were labeled with anti-Myosin 7a (1:500, 25–6790, Proteus-biosciences) and quantified under a 63× objective field.

Choline acetyltransferase (ChAT) and tyrosine hydroxylase (TH) quantification and localization: The basilar membrane of the cochlea was divided into three turns, labeled with ChAT (1:500, AB144P, Millipore), TH (1:100, 58844, Cell Signaling Technology), and phalloidin (1:2000, A30104, ThermoFisher). Images were observed in a 40×objective field and analyzed using ImageJ for volume measurement and colocalization analysis.

2.7. Statistical analysis

Data analysis was conducted using Microsoft Excel and GraphPad Prism version 8. Detailed statistical information is provided in the results section, figures, and figure legends. All data are presented as mean ± standard error of the mean (SEM). Statistical significance was determined using two-tailed unpaired *t* tests and two-way ANOVA followed by Sidak's multiple

comparisons test, as indicated in each figure. The exact values of *n* are provided where appropriate. *, **, ***, **** indicate $p < 0.05$, 0.01, 0.001, and 0.0001, respectively.

3. Results

3.1. No significant differences were observed in hearing and corresponding morphology between PD and control mice

The MPTP mouse model is widely used in PD pathogenesis (*18-22*). We established a PD mouse model according to the experimental protocol in Supplementary Figure S1 A, *https://www.biosciencetrends.com/action/getSupplementalData.php?ID=279*, and verified by behavioral and morphological assessments. In detail, mice with abnormal hearing were excluded, and remaining mice were randomly assigned to two groups: the MPTP group (model group), which received intraperitoneal injections of MPTP-HCl once daily for 5 days, while the control group received an equivalent volume of saline *via* intraperitoneal injection once daily for 5 days (*18-22*). Subsequent experiments were conducted according to the experimental protocol without a time interval. Mice in two groups underwent behavioral testing, open field test, and audiological assessment, ABR and DPOAE, followed by tissue collection for pathological examination of the brain and cochlea immediately. Based on the successful establishment of the PD model, confirmed by behavioral and pathological analyses, findings regarding audiology and cochlear morphology were obtained (Supplementary Figure S1 A, *https://www.biosciencetrends.com/action/getSupplementalData.php?ID=279*). As shown in Supplementary Figure S1 B-C (*https://www.biosciencetrends.com/action/getSupplementalData.php?ID=279*), MPTP-treated mice exhibited significantly impaired locomotor activity. Immunofluorescence and immunohistochemistry both revealed a significant reduction in dopaminergic neurons in the substantia nigra of PD mice compared to controls (Supplementary Figure S1 D-E, *https://www.biosciencetrends.com/action/getSupplementalData.php?ID=279*). Therefore, we confirmed the successful establishment of the PD mouse model. To assess hearing differences between control and PD mice, we performed ABR and DPOAE testing. As shown in Figure 1A and B, ABR and DPOAE thresholds did not differ significantly between groups. Notably, compared to the control group, the PD group exhibited a mild increase in DPOAE threshold at 32 kHz, although it was not significant. Next, we focused on the latency and amplitude of ABR wave I (Figure 1 C-D). No significant change in wave I latency was found between groups, but amplitude was lower in the PD group, though this difference was not significant. Notably, compared with other frequencies, the wave I amplitude gap between the PD and control group was much smaller at 32 kHz. Next, we labeled hair cells with phalloidin to assess the impact of modeling on hair cell survival (Figure 1 E-F). Results showed no significant difference in inner and outer hair cell survival between groups (Figure 1 G-H). And ribbon synapse labeled by Ctbp2 shown in Figure 2 I-J also exhibited no dramatic numbers change at all turns between groups, although in the middle and base turn, PD mice exhibited a mild reduction in synapse numbers with no significance. Interestingly, compared with regular distribution in the basal turn, synapses in the apical and medial regions seemed more disorganized.

3.2. $ChAT^+$ fibers in the PD mice cochlea exhibited post-injury compensatory changes

Then we labeled ChAT in hair cells. The results showed that $ChAT^+$ regions exhibited increased total fluorescence intensity, enlarged volume, and heightened average fluorescence intensity across the entire cochlear hair cell (Figure 2 D-F). Furthermore, $ChAT^+$ hair cell segments exhibited more pronounced increases in total fluorescence intensity and volume at the mid-basal transition region, while the mean fluorescence intensity of the $ChAT^+$ hair cell fraction showed a more pronounced increase in the apical-medial turn. Next, we performed quantitative analysis of the $ChAT^+$ portion in inner hair cells. We found that the total fluorescence intensity, total volume, and average fluorescence intensity of the inner hair cell portion also increased. The total fluorescence intensity and volume of the $ChAT^+$ inner hair cell portion in the apical and basal turns appeared to increase more significantly. At the level of individual inner hair cells (Supplementary Figure S3 A-C, *https://www.biosciencetrends.com/action/getSupplementalData.php?ID=279*), $ChAT^+$ total fluorescence intensity, total volume, and average fluorescence intensity changes were similar to the entire $ChAT^+$ inner hair cell segment. Subsequently, we performed fluorescence quantification analysis on the $ChAT^+$ portions in outer hair cells (Figure 2 K-M). Likewise, we found that the total fluorescence intensity, total volume, and average fluorescence intensity remained increased in the PD group, with a much more pronounced increase in the mid-basal turn. At the level of individual outer hair cells (Supplementary Figure S3 D-F, *https://www.biosciencetrends.com/action/getSupplementalData.php?ID=279*), these analyses were also similar to overall outer hair cell $ChAT^+$ segment alterations. Notably, although the $ChAT^+$ portion in the hair cell region of the PD model seemed much more activated, its distribution appeared more disorganized, particularly on the apical and basal turns (Figure 2 A-C).

3.3. TH^+ fibers showed heterogeneous alterations in the PD mouse cochlea

TH, commonly used to label the morphology and short-term dopaminergic neuronal activity of dopamine

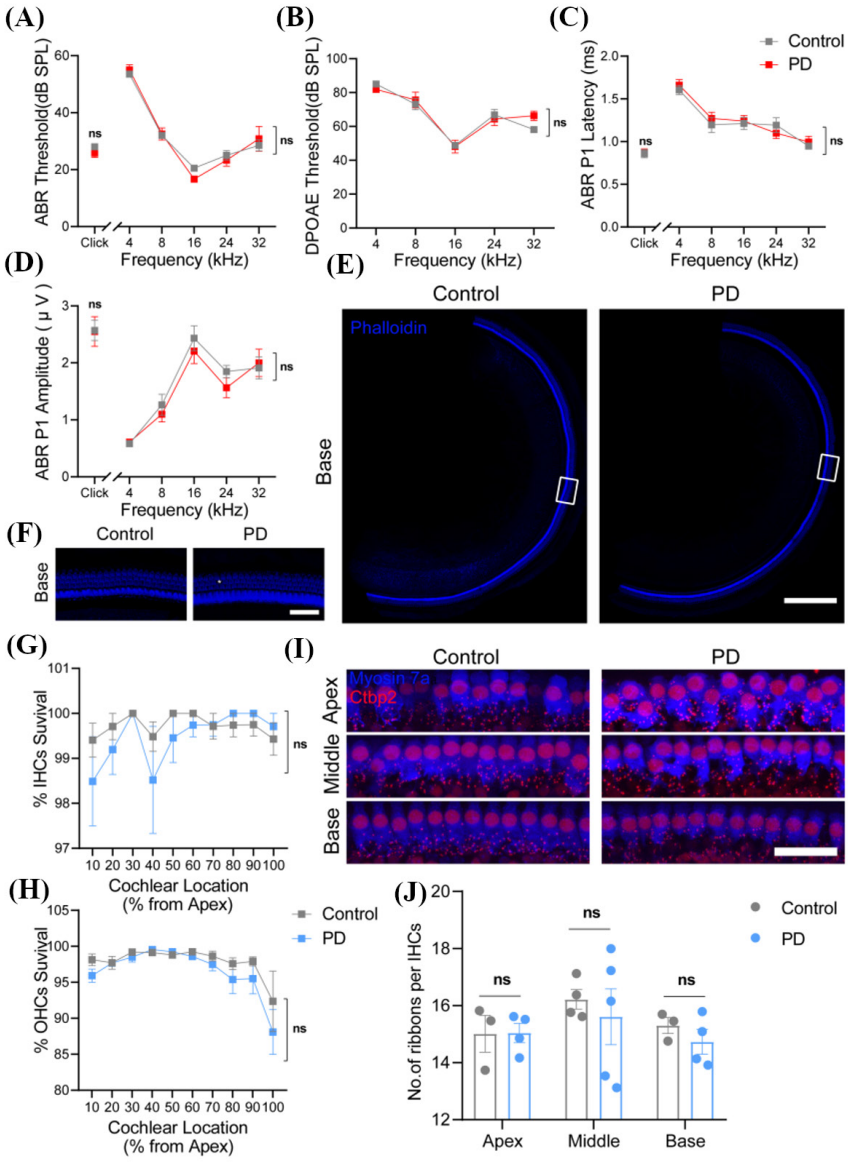

Figure 1. No significant differences were observed in hearing and corresponding morphology between PD and control mice. (A-D) Audiometric testing of control and PD mice: **(A)** showed ABR (control, *n* = 10; pd, *n* = 6); **(B)** showed DPOAE (control, *n* = 8; pd, *n* = 8); **(C)** showed ABR wave 1 latency (control, *n* = 10; pd, *n* = 6); **(D)** showed ABR wave 1 amplitude (control, *n* = 10; pd, *n* = 6). (E-H) Cochlear hair cell analysis in control and PD mice: **(E)** showed survival of basal turn hair cells, with blue labeling for phalloidin, bar = 250 μm; **(F)** was a magnification of the region in E, bar = 40 μm; **(G)** presented quantitative analysis of inner hair cells in both groups (control, *n* = 5; pd, *n* = 5); **(H)** presented quantitative analysis of inner and outer hair cells in both groups (control, *n* = 5; pd, *n* = 5). (I-J) Detection of ribbon synapses in inner hair cells of control and PD mice: **(I)** showed representative images of apical, middle, and basal turns in both groupsl; blue indicated Myosin 7a, red indicated Ctbp2, bar = 30μm; **(J)** showed quantitative analysis of apical, middle, and basal turns in both groups. Results are presented as mean ± SEM; ns indicates no significance. Two-way ANOVA followed by Sidak's multiple comparisons test.

fibers, can also mark the morphology and activity of noradrenergic fibers (*27*). TH^+ fibers in the cochlea are usually classified into dopaminergic fibers situated in the inner hair cell region and adrenergic sympathetic fibers located in the OSL (*28*). Our results showed that dopamine fiber distribution significantly decreased in the apical-middle region of the PD group, while it significantly increased in the basal turn (Figure 3B), which was verified by quantitative analysis in Figure 3 C-E. However, the average fluorescence intensity of the TH^+ region was significantly reduced, particularly in the basal turn. And in the OSL, for the first time, we observed significant reductions both in total fluorescence intensity, total volume, and average fluorescence intensity in the TH^+ region, particularly in the mid-basal turn (Figure 3A and F-H). Next, we focused on the colocalization between cholinergic and dopaminergic neurons in the inner hair cell region. The results (Figure 3 I-K) showed that PD modeling significantly altered the colocalization between them, and a marked increase was evident in the basal turn.

3.4. PD model mice exhibited heightened sensitivity to low-to-moderate noise intensity

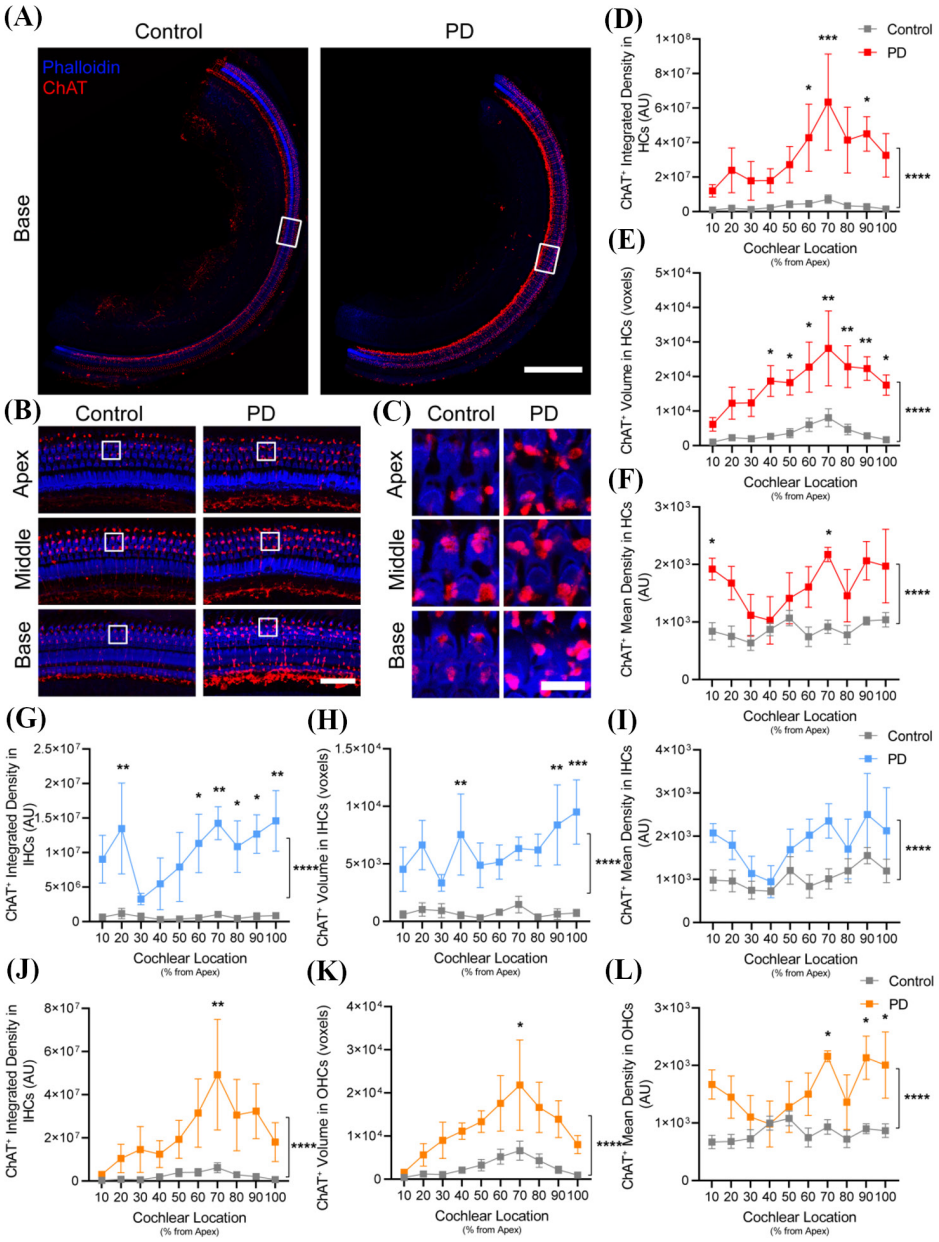

Figure 2. ChAT$^+$ fibers in PD mice cochlea exhibited post-injury compensatory changes. (A) showed the ChAT$^+$ portion of the basal turn, with blue labeling for Phalloidin and red labeling for ChAT, bar = 250 μm. **(B)** displayed the change of ChAT$^+$ portion in apical, middle, and basal turn, bar = 40 μm. **(C)** showed a magnified view of B, bar = 10 μm. **(D)(E)(F)** presented quantitative analysis of ChAT$^+$ portion in hair cells, corresponding to integrated density, volume, and mean density, respectively. **(G)(H)(I)** quantitative analysis of ChAT$^+$ portion in inner hair cells, corresponding to integrated density, volume, and mean density, respectively. **(J)(K)(L)** quantitative analysis of ChAT$^+$ portion in outer hair cells, corresponding to integrated density, volume, and mean density, respectively (control, $n = 5$; PD, $n = 4$). Results are presented as mean ± SEM. *$p < 0.05$, **$p < 0.01$, ***$p < 0.005$, ****$p < 0.0001$. Two-way ANOVA followed by Sidak's multiple comparisons test.

Based on our research (*29*), we exposed both groups to 108 dB SPL white noise for 2 hours. ABR and DPOAE tests were conducted at day 1, 3, and 7 post-noise exposure to investigate hearing changes (Figure 4A). Our results revealed that at day 1 post-noise exposure, the PD group exhibited significant ABR threshold shifts compared to the control group in all frequencies, and much pronounced on clicks and 16 kHz (Figure 4B). By day 3, this gap gradually narrowed (Figure 4C), and on day 7 post-noise exposure, shift differences still existed between groups, although a significant gap was observed only in the high-frequency range (Figure 4D). But in DPOAE results, no significant differences were found, although the overall threshold shift gap between groups mirrored that of ABR (Figure 4 E-G). Interestingly, at 3 days post-noise exposure, the threshold shift at 32 kHz was much lower in the control group. And then, we examined changes in ABR wave 1 latency and amplitude (Figure 4 H-M). The PD group exhibited increased ABR wave 1 latency and decreased ABR wave 1 amplitude. Interestingly, the latency of ABR wave 1 showed no significant change at 32 kHz.

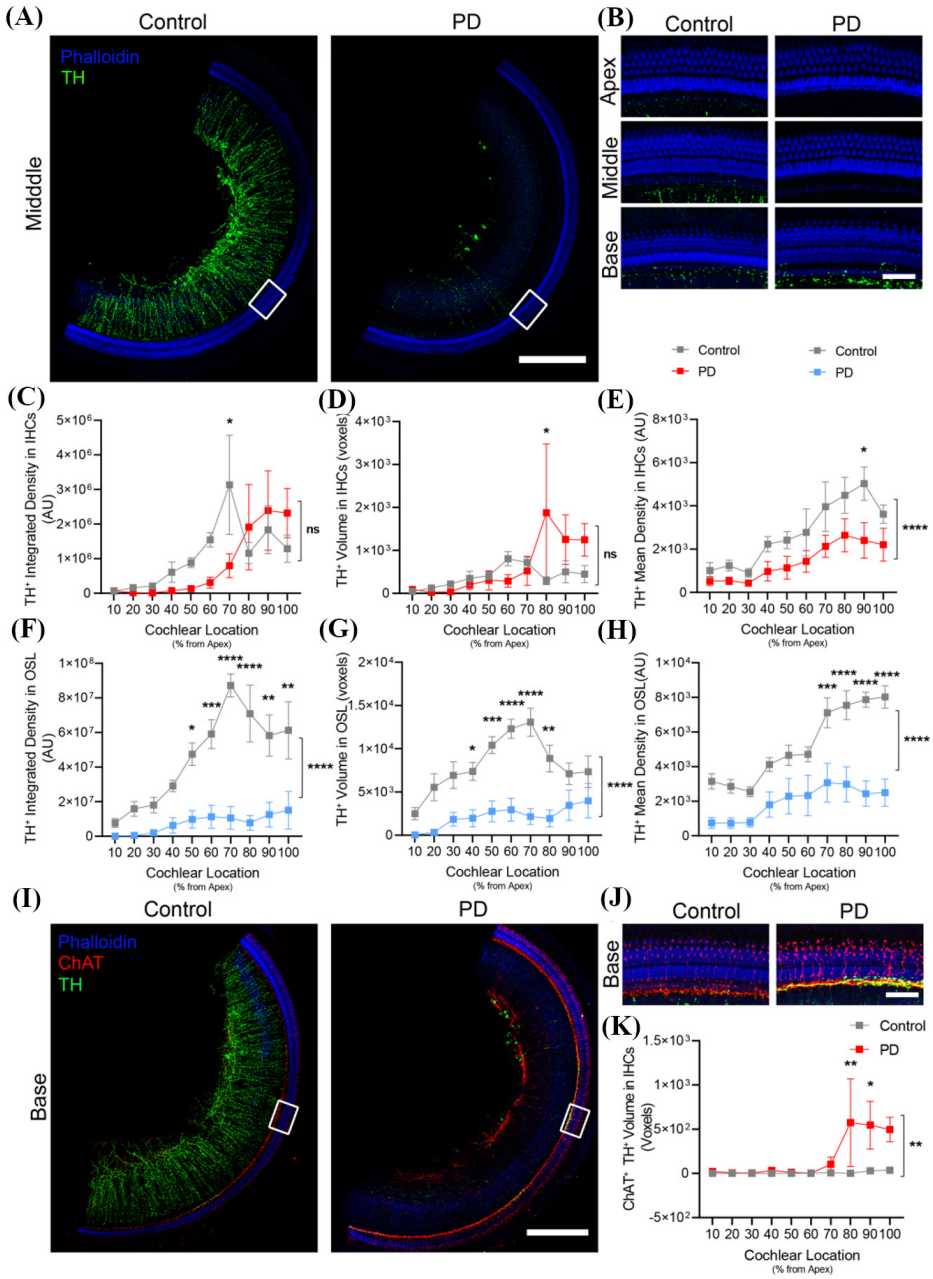

Figure 3. TH$^+$ fiber alterations in PD mouse models. (A) showed that the middle turn TH$^+$ region primarily displays sympathetic fibers in the medial spiral plate. Blue staining indicates Phalloidin, green staining indicates TH. Bar = 250 μm. **(B)** displayed the change of dopamine fibers in apical, middle, and basal turns, bar = 40 μm. **(C)(D)(E)** presented quantitative analyses of the inner hair cell TH$^+$ region, corresponding to integrated density, volume, and mean density, respectively. **(F)(G)(H)** presented quantitative analysis of the OSL TH+ region, corresponding to integrated density, volume, and mean density, respectively (control, $n = 6$; PD, $n = 5$). **(I)** showed the colocalization of ChAT$^+$ and TH$^+$ in the basal turn. Blue labeling indicated Phalloidin, red labeling indicated ChAT, and green labeling indicated TH. Bar = 250 μm. **(J)** showed a magnified view of a close-up of panel I. bar = 40 μm. **(K)** spatial co-localization analysis of ChAT$^+$ and TH$^+$ inner hair cell regions across the entire cochlea (control, $n = 5$; PD, $n = 4$). Results are presented as mean ± SEM. ns, no significance. *$p < 0.05$, **$p < 0.01$, ***$p < 0.005$, ****$p < 0.0001$. Two-way ANOVA followed by Sidak's multiple comparisons test.

3.5. PD rats demonstrated alterations in auditory function and corresponding morphology

Based on prior studies, we introduced the Sprague-Dawley rats' PD model (*23-26*). We established a PD rat model according to the experimental protocol in Figure S3A and B, and verified it by behavioral and morphological assessments. In detail, SD rats were screened for hearing abnormalities and excluded as described previously (*23-26*). Rats underwent unilateral 6-OHDA lesions of the substantia nigra pars compacta (SNc). Control rats received an equivalent injection of physiological saline containing 0.02% ascorbic acid (*23-26*). Subsequent procedures were performed according to the experimental protocol after 3 weeks. Both groups of rats underwent behavioral testing, open field test, and

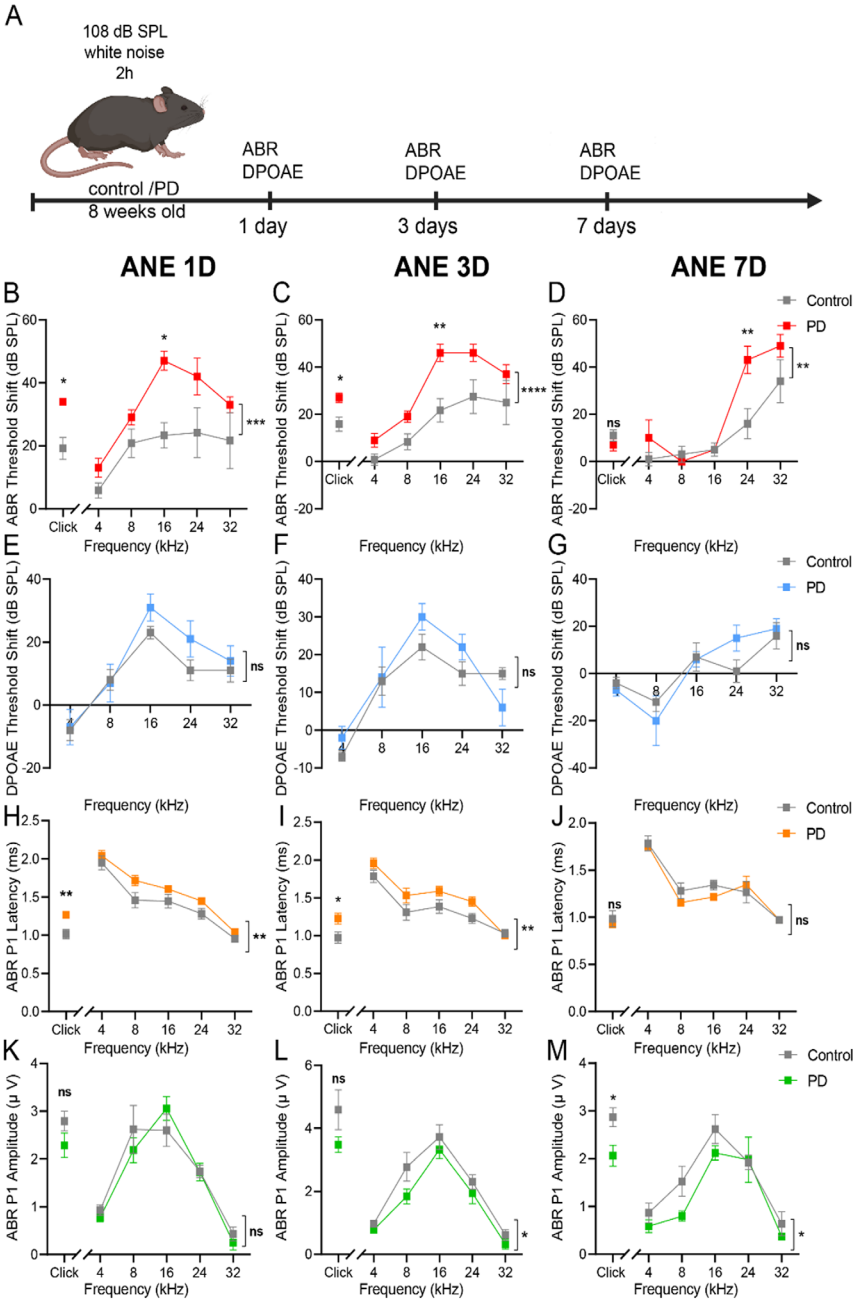

Figure 4. PD model mice exhibited heightened sensitivity to low-to-moderate noise intensity. (A) Schematic of auditory sensitivity testing. Control and PD mice underwent ABR and DPOAE testing at days 1, 3, and 7 post-exposure to 108 dB broadband white noise. **(B)(C)(D)** ABR recordings. **(H)(I)(J)** ABR L1 latency measurements. **(K)(L)(M)** ABR L amplitude measurements, (ANE 1D, control, $n = 6$; PD, $n = 5$) (ANE 3D, control, $n = 6$; PD, $n = 5$) (ANE 7D, control, $n = 5$; PD, $n = 5$). **(E)(F)(G)** DPOAE measurements (ANE 1D, control, $n = 5$; PD, $n = 5$) (ANE 3D, control, $n = 5$; PD, $n = 5$) (ANE 7D, control, $n = 5$; PD, $n = 5$). Results are presented as mean ± SEM. $*p < 0.05$, $**p < 0.01$. Two-way ANOVA followed by Sidak's multiple comparisons test.

audiological assessment, ABR and DPOAE, followed by tissue collection for pathological examination of the brain and cochlea immediately. Based on the successful establishment of the PD model, confirmed by behavioral and pathological analyses, findings regarding audiology and cochlear morphology were obtained (Supplementary Figure S2 A, *https://www.biosciencetrends.com/action/getSupplementalData.php?ID=279*). As shown in the results, 6-OHDA-injected rats revealed significantly impaired locomotor activity (Supplementary Figure S2 C-D, *https://www.biosciencetrends.com/action/getSupplementalData.php?ID=279*). Correspondingly, immunofluorescence and immunohistochemical analysis both revealed a significant reduction in dopamine neurons in the injected side of the substantia nigra in PD rats (Supplementary Figure S2 E-F, *https://www.biosciencetrends.com/action/getSupplementalData.php?ID=279*). Thus, we confirmed the successful establishment of the PD rat model. Considering potential bilateral effects resulting from unilateral destruction of dopamine neurons in the substantia nigra (*30,31*), we analyzed auditory and morphological parameters on

the ipsilateral and contralateral sides of PD model rats, respectively. As shown in Figure 5A, ABR thresholds in both the surgical and contralateral sides of the PD group were significantly higher than those in the control group, and similar trends were shown in DPOAE thresholds (Figure 5B). Next, we examined changes in ABR I latency and amplitude (Figure 5 C-D). Compared to the control group, both the ipsilateral and contralateral sides in the PD group exhibited prolonged latencies and reduced amplitudes significantly, in agreement with the ABR threshold shifts. Subsequently, morphological analysis among the three groups was conducted, and phalloidin staining results (Figure 5 E-H) showed no significant differences in inner hair cell survival among the three groups. However, outer hair cell survival in the control group was significantly better than in both the ipsilateral and contralateral sides of the PD group, particularly at the 10% from apex and 100% from apex positions, while the contralateral side of the PD group showed significantly reduced outer hair cell survival compared to the control group. Subsequently, we labeled the ribbon synapse, as shown in Figure 5

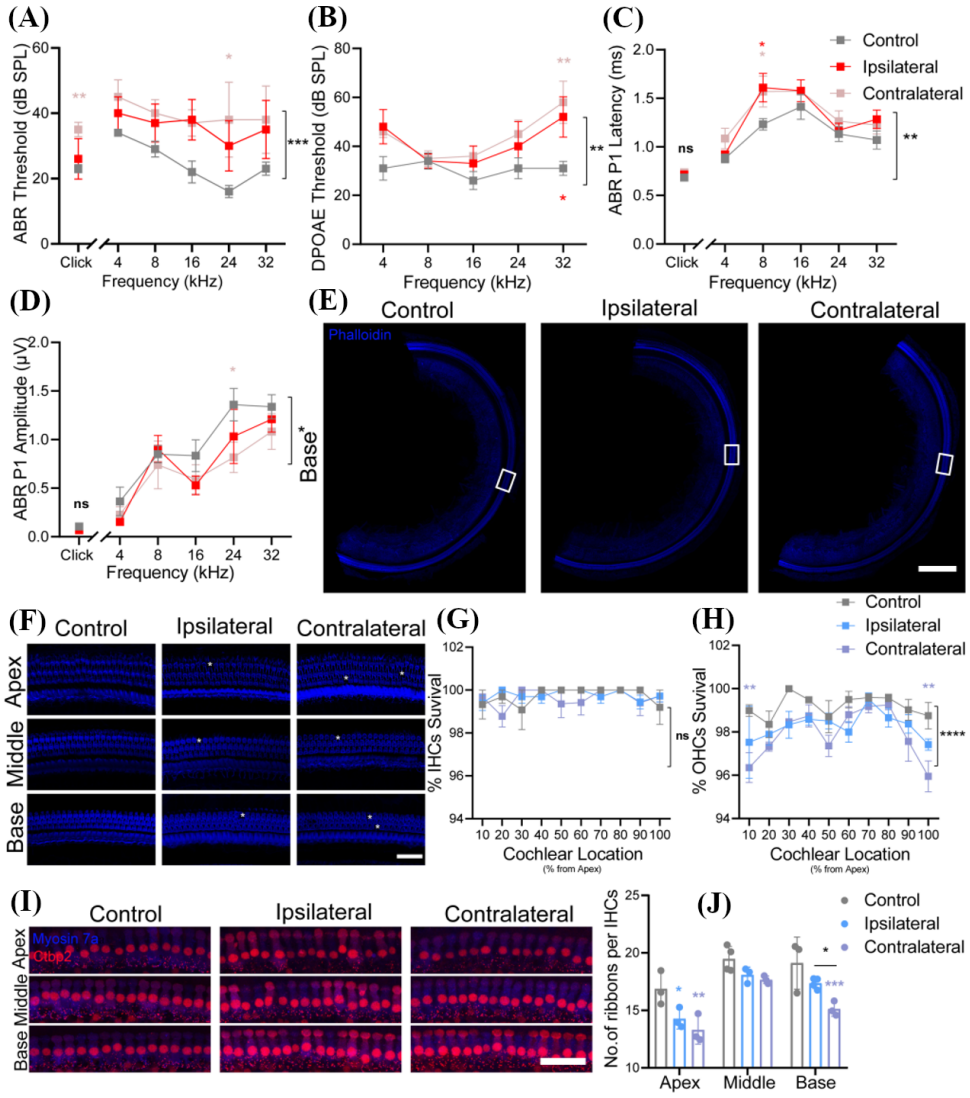

Figure 5. PD rats demonstrated alterations in auditory function and corresponding morphology. (A-D) Audiological testing of control rats and PD rats on the ipsilateral and contralateral sides: **(A)** showed ABR (control group, n = 5; ipsilateral, n = 5; contralateral, n = 5). **(B)** showed DPOAE (control group, n = 5; ipsilateral, n = 5; contralateral, n = 5). **(C)** showed ABR L1 latency (control group, n = 5; ipsilateral, n = 5; contralateral, n = 5). **(D)** showed ABR L1 amplitude (control group, n = 5; ipsilateral, n = 5; contralateral, n = 5). (E-H) Cochlear hair cell assessment in PD and control mice: **(E)** showed survival of basilar hair cells, with phalloidin labeled in blue, bar = 300 μm. **(F)** was a magnified section of E, bar = 40 μm. **(G)** presented quantitative analysis of inner hair cells in both groups (control, n = 4; ipsilateral, n = 4; contralateral, n = 4). **(H)** presented quantitative analysis of outer hair cells in both groups (control, n = 4; ipsilateral, n = 4; contralateral, n = 4). (I-J) Ribbon synapses detection in inner hair cells of PD and control mice: **(I)** showed representative images of apical, middle, and basal turns in both groups, with blue labeling for Myosin 7a and red for Ctbp2, bar = 10 μm. **(J)** presented quantitative analysis of apical, middle, and basal turns in both groups. Pink and purple p-values represented comparisons between the control group and the contralateral group, red P-values indicated comparisons between the control group and the ipsilateral group. Results are presented as mean ± SEM. ns, no significance. *p < 0.05, **p < 0.01, ***p < 0.005, ****p < 0.0001. Two-way ANOVA followed by Sidak's multiple comparisons test.

I-J, among the three groups, synapses at the apical, middle, and basal turns exhibited a stepwise decrease, and this reduction was more pronounced at the apical and basal turns. Notably, the number of synapses on the contralateral side was significantly lower than the control group at both apical and basal turns, coordinated with the absence of outer hair cells. Interestingly, no significant differences were observed in the arrangement of synapses or the morphology of inner hair cells among the three groups.

3.6. $ChAT^+$ fibers in PD rats displayed asymmetric alterations

We labeled the $ChAT^+$ portions of hair cells in the control group, the PD group's surgical side, and the contralateral side. Results showed that the total intensity of $ChAT^+$ portions in hair cells on both the operated and contralateral sides was higher than in the control group, and their distributions were not consistent bilaterally, although lacking statistical significance. And no significant differences were observed in the volumes of the three groups. Regarding mean fluorescence intensity, both the operated and contralateral sides were significantly higher than the control group, especially in the apical and basal regions, the contralateral side exhibited higher intensity than the operated side, although with no statistical significance (Figure 6 D-F). Next, we investigated ChAT expression in inner hair cells. The trends for total and average fluorescence intensity in the inner hair cell region were similar to the entire hair cells. However, the volume of both the ipsilateral and contralateral sides was higher than the control group, and the distribution of the two sides was inconsistent but not significant (Figure 6 G-I). In the level of individual inner hair cells, the changes in $ChAT^+$ total fluorescence intensity, total volume, and mean fluorescence intensity were similar to those observed in the entire $ChAT^+$ inner hair cell part (Supplementary Figure S2 A-C, *https://www.biosciencetrends.com/action/getSupplementalData.php?ID=279*). And in the outer hair cell region, total fluorescence intensity and average fluorescence intensity on both the surgical and contralateral sides of the PD group were mildly higher, while the overall volume was lower than the control group, but insignificant compared with the $ChAT^+$ region in inner hair cells (Figure 6 J-L). And individual outer hair cells showed similar results (Supplementary Figure S4 D-F, *https://www.biosciencetrends.com/action/getSupplementalData.php?ID=279*). Overall, the expression of ChAT exhibited asymmetric changes in both sides of PD rats, with more pronounced alterations in average fluorescence intensity, especially in the inner hair cell part. Furthermore, similar to the findings in mice, its distribution within inner and outer hair cells appeared more disorganized in the PD rat cochlea (Figure 6 A-C).

3.7. TH^+ fibers revealed asymmetric alterations in the PD rat model

Then, we labeled dopaminergic neurons in the inner hair cell region and adrenergic sympathetic fibers in the OSL region using TH labeling. As shown in Figure 7 B-E, no significant differences were observed in the total fluorescence intensity or volume of TH^+ regions within the inner hair cell area among the groups. However, in the region 70% from the apex, the total fluorescence intensity in the PD group's ipsilateral and contralateral sides was higher than the control group, with significance observed only between the PD group's ipsilateral side and the control group. Regarding total volume, the PD group's contralateral side significantly exceeded both the control group and the operated side. In terms of average fluorescence intensity, both the surgical and contralateral sides of the PD group exhibited higher values compared to the control group. However, the relationship among the three groups was not uniform. In the region 40–50% from the apex, the average TH fluorescence intensity on the contralateral side of the PD group was significantly higher than the control group. Conversely, in the regions 70–90% from the apex, the PD group's operated side showed higher TH average fluorescence intensity than the control group, where the changes in the PD group's contralateral side tended toward the control group's values. Next, we examined the TH^+ fraction in the OSL region (Figure 7A and F-H). Results revealed no significant differences in total intensity or volume among the three groups in the regions 10–60% from the apex. However, in the 60–100% region, the control group, the PD contralateral side, and the PD surgical side exhibited a stepwise decrease, with volume showing a significant reduction. Nevertheless, no significant differences were observed in mean fluorescence intensity among the three groups. In contrast, changes in the TH^+ region exhibited more complex characteristics in the 6-OHDA rat model group. Subsequently, we examined co-localization between $ChAT^+$ and TH^+ parts in the inner hair cell region of rats. Results revealed that PD modeling reduced co-localization probability, particularly in the region 70% from the apex, where the PD group's surgical side showed significantly lower levels than the control group. At this point, the PD group also showed significantly lower levels on the operated side compared to the contralateral side. Although the contralateral side in the PD group was lower than the control group, the difference was not statistically significant. However, notably, compared to mice, the overall colocalization voxels in the rat model were not high (Figure 7 I-K).

4. Discussion

Growing evidence suggests that hearing loss, as a non-motor sensory impairment in PD, may serve as an indicator of progression and treatment response (*32*).

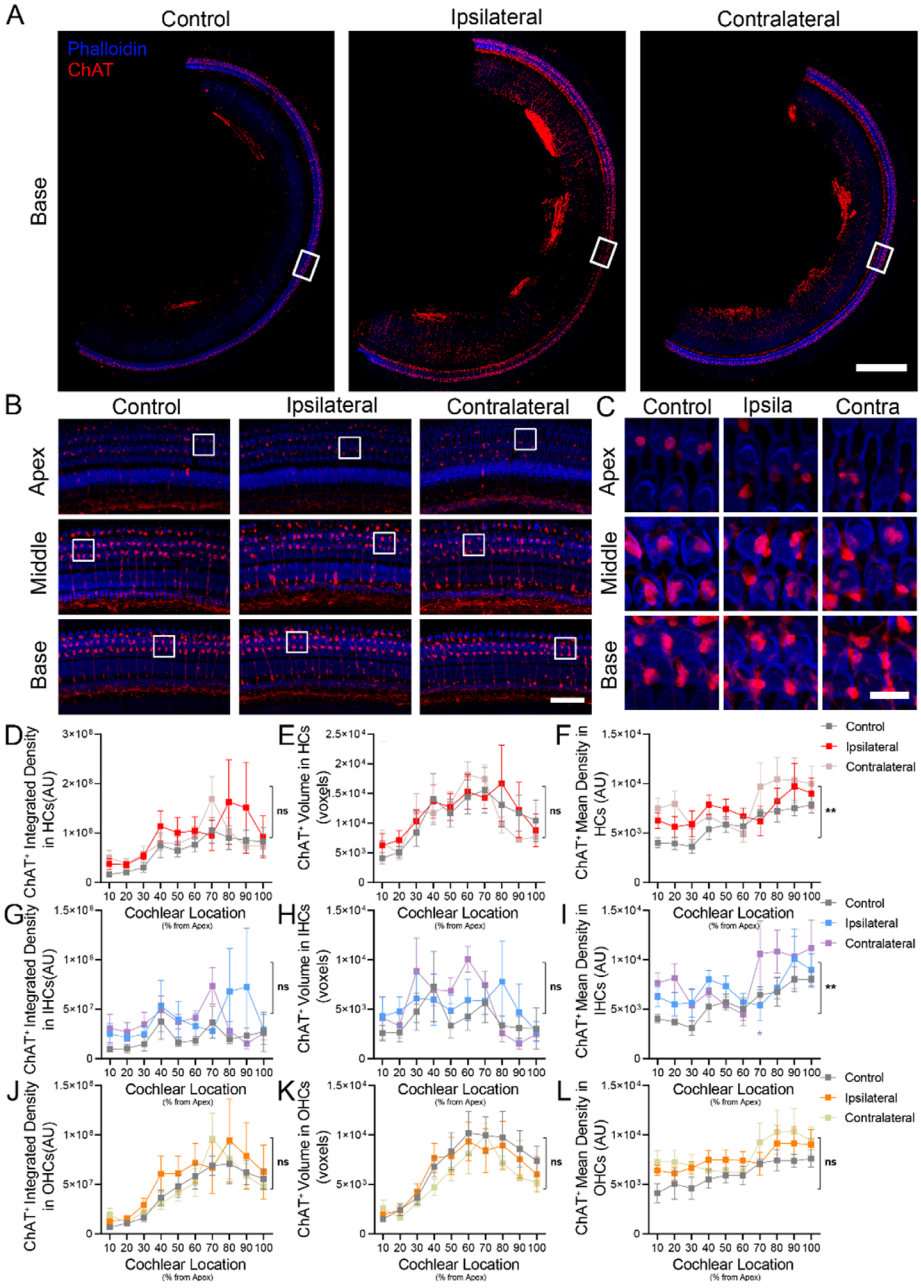

Figure 6. ChAT$^+$ fibers in PD rats displayed asymmetric alterations. (A) showed the ChAT$^+$ portion of the basal turn, with blue labeling for Phalloidin and red labeling for ChAT, bar = 300 μm. **(B)** displayed the change of ChAT$^+$ portion in apical, middle, and basal turn, bar = 40 μm. **(C)** is a magnification of panel B, bar = 10 μm. **(D)(E)(F)** presented quantitative analysis of ChAT$^+$ portion in hair cells, corresponding to integrated density, volume, and mean density, respectively. **(G)(H)(I)** quantitative analysis of ChAT$^+$ portion in inner hair cells, corresponding to integrated density, volume, and mean density, respectively. **(J)(K)(L)** quantitative analysis of ChAT$^+$ portion in outer hair cells, corresponding to integrated density, volume, and mean density, respectively (control, $n = 4$; ipsilateral, $n = 4$; contralateral, $n = 4$). Purple p-values represented comparisons between control and contralateral groups. Results are presented as mean ± SEM. ns, no significance. *$p < 0.05$, **$p < 0.01$. Two-way ANOVA followed by Sidak's multiple comparisons test.

However, studies on peripheral, particularly cochlear, pathological manifestations and mechanisms in PD models remain scarce. Therefore, this work primarily focuses on hearing changes and cochlear pathology in PD models, aiming to provide new insights into the mechanisms and treatment of hearing alterations in PD.

MPTP, a neurotoxin commonly used to induce PD models, selectively targets dopaminergic neurons (*33*). Previous studies demonstrated that MPTP significantly alters auditory measures such as ABR and category of auditory performance (CAP), causes marked damage to central auditory structures, including the inferior colliculus and lateral colliculus, and severely disrupts the echolocation system in bats (*34,35*). However, in our current study, MPTP-treated mice exhibited no clear alterations in ABR or DPOAE, while no significant loss of inner or outer hair cells was observed, hinting that MPTP exposure alone may be insufficient to induce pronounced peripheral auditory dysfunction in our PD mice. Ribbon synapses, the critical structures that

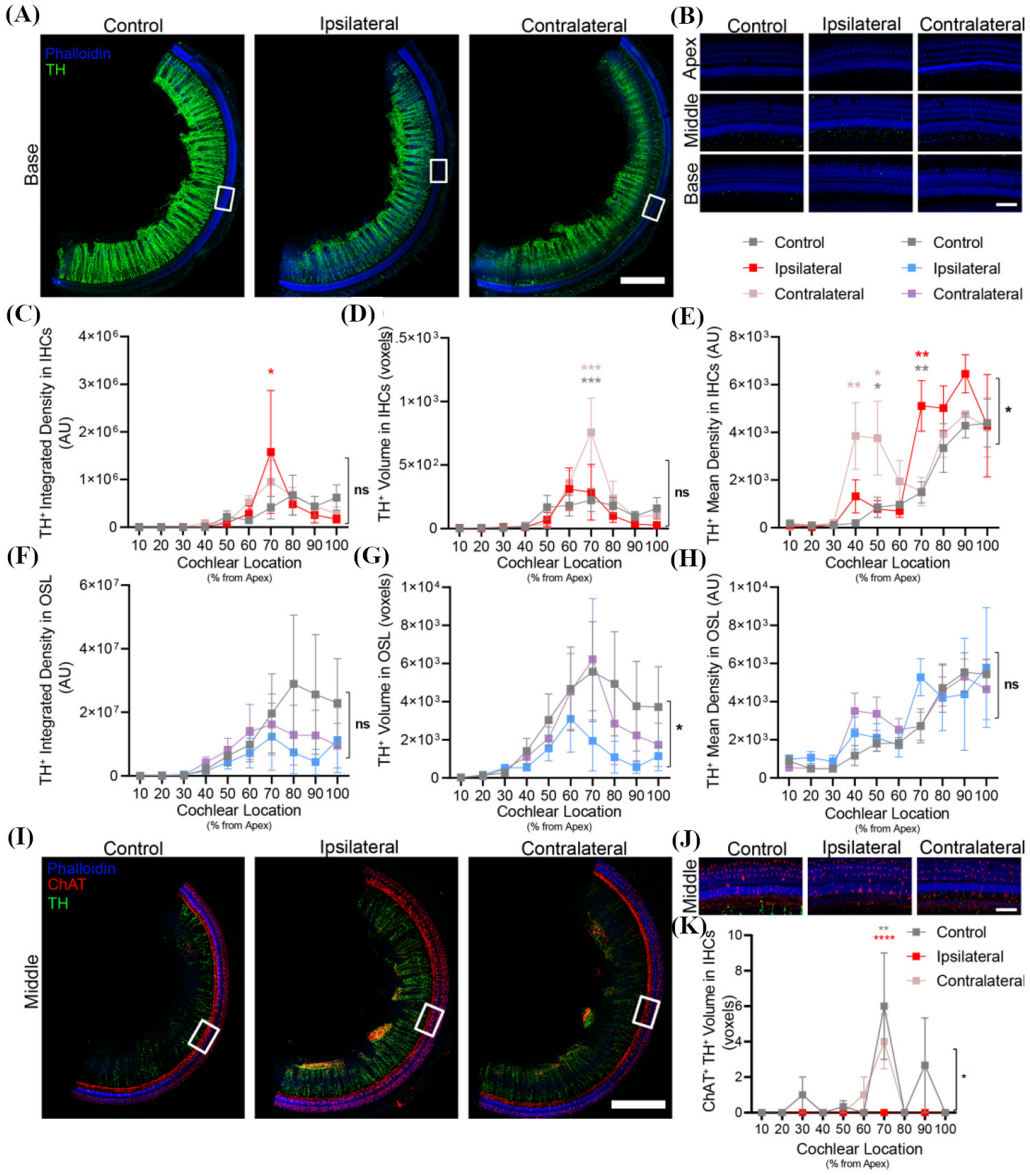

Figure 7. TH$^+$ fibers revealed asymmetric alterations in the PD rat model. (A) The middle turn TH$^+$ region primarily displays sympathetic fibers in the medial spiral plate. Blue staining indicates Phalloidin, green staining indicates TH. bar = 300 μm. **(B)** displayed the change of dopamine fibers in apical, middle, and basal turns, bar = 40 μm. **(C)(D)(E)** presented quantitative analyses of the inner hair cell TH$^+$ region, corresponding to integrated density, volume, and mean density, respectively. **(F)(G)(H)** presented quantitative analysis of the OSL TH$^+$ region, corresponding to integrated density, volume, and mean density, respectively (control, n = 3; lpsilateral, n = 3; contralateral, n = 3). **(I)** showed the colocalization of ChAT$^+$ and TH$^+$ in the middle turn. Blue labeling indicated Phalloidin, red labeling indicated ChAT, and green labeling indicated TH. bar = 300 μm. **(J)** showed a magnified view of a close-up of panel. bar = 40 μm. **(K)** Spatial co-localization analysis of ChAT$^+$ and TH$^+$ inner hair cell regions across the entire cochlea (control, n = 3; ipsilateral, n = 3; contralateral, n = 3). Red p-values indicated comparisons between the control and ipsilateral groups. Gray p-values indicated comparisons between the ipsilateral and contralateral groups. Results are presented as mean ± SEM. ns, no significance. *$p < 0.05$, **$p < 0.001$, ***$p < 0.005$. Two-way ANOVA followed by Sidak's multiple comparisons test.

transmit signals from inner hair cells to afferent neurons, are known to exhibit early pathological changes that precede alterations in ABR, DPOAE thresholds, and hair cell survival, particularly in hidden hearing loss (*36*). Notably, our study found no significant loss of synapses in all turns. Consistently, the latency and amplitude of the ABR 1 wave showed no obvious changes compared to controls. Interestingly, despite no clear numerical change, the synapses at the basal turn exhibited greater regularity relative to those at the apical and middle turns. Correspondingly, the ABR wave 1 amplitude at 32 kHz remained largely unchanged compared to 8 kHz and 16 kHz. These findings suggest that MPTP did not specifically target hair cells or synapses to cause significant damage. Interestingly, previous studies have found a higher proportion of functional hearing loss among PD patients, where no significant differences in pure-tone audiometry (PTA) abnormalities were observed (*37*).

The LOC and MOC systems, as efferent components of the auditory pathway, play a critical role in auditory sensitivity and discrimination. Alterations in these

systems often precede hair cells and ribbon synapses (*38*). In our PD models, ChAT-labeled cholinergic neurons exhibited a marked increase in both fiber volume and ChAT expression levels, indicating enhanced cholinergic activity, which may reflect secondary or compensatory mechanisms. Moreover, we noted more disorganized ChAT distribution at the apical and basal turns, further indicating that compensatory activity of cholinergic fibers is possibly dysregulated. Interestingly, previous studies involving MPTP injection into the guinea pig round window showed no significant changes in MOC volume. However, this study primarily focuses on MPTP's toxicological effects rather than its potential damage to the systemic motor and non-motor systems as a PD model inducer (*35*).

As a key component of the cochlear LOC, dopaminergic neurons primarily coordinate with cholinergic neurons in the LOC to encode sound localization in inner hair cells. Previous studies indicated that dopaminergic neurons in the LOC may form synaptic structures with auditory afferents, inhibiting the excitability of auditory afferent electrical activity (*11*). To date, no studies have focused on their potential alterations in PD models. We report, for the first time, that dopamine fibers in the apical and middle turn are significantly depleted in the MPTP model. Therefore, we hypothesize that loss of dopaminergic fibers disrupts inhibitory control within the LOC circuitry, leading to compensatory activation of cholinergic neurons; however, as we have seen, this activation is not perfect, which failed to shield inner hair cells and synapses from the risk of glutamate toxicity caused by an abnormal increase in afferent signals. Consequently, the body rapidly but imperfectly activates the MOC efferent system, the myelinated fiber, to inhibit the excitability of outer hair cells and reduce the intensity of sound signal input, ultimately protecting inner hair cells and synaptic structures (*10*). Interestingly, beaded enlargements of dopaminergic fibers were observed at the basilar turn of the cochlea. However, it remains unclear whether these swollen dopaminergic neurons retain partial functionality. Notably, dopaminergic and cholinergic neurons show marked co-localization increases in the basilar turn. Previous studies also suggest their increased overlap after noise exposure (*13,27*), though their precise significance remains unclear. Interestingly, we observed a marked loss of adrenergic sympathetic innervation in the OSL for the first time. Similar denervation of sympathetic fibers has been observed in cortical and cardiac tissues of MPTP-induced PD monkey models (*39,40*). This absence may result from the secondary consequences of dopaminergic degeneration in the substantia nigra. Numerous studies have demonstrated concomitant sympathetic fiber pathology in PD patients (*41,42*). In the cochlea, sympathetic fibers in the OSL primarily regulate vascular tone supplying hair cells and afferent/efferent nerves (*43*). Following sympathetic denervation, the loss of vascular tone may leave the hair cells and afferent/efferent nerves in a relatively ischemic state; however, its specific role in hearing remains unclear.

Based on these findings and prior research, we hypothesized that our MPTP-induced mouse model primarily caused damage in auditory sensitivity (*44*). Therefore, we exposed PD mouse models to low-to-moderate intensity noise. Noise exposure for 1, 3, and 7 days resulted in significant fluctuations in ABR thresholds, P1 latency, and amplitude, while DPOAE exhibited no significant change, suggesting that outer hair cells may not have sustained substantial damage. These findings validate our hypothesis that in our mouse model, hearing impairment primarily manifested as changes in auditory sensitivity resulting from the loss of compensation in the LOC and MOC. We also observed that, compared to other frequencies, the amplitude of fluctuations at 32 kHz was not significantly affected by low-to-moderate noise exposure, particularly evident in ABR P1 latency. This suggested that the beaded dopamine neurons located at the basilar turn, identified in our results, may retain partial compensatory capacity. Interestingly, previous studies on cholinergic neurons in auditory sensitivity have shown that enhancing cholinergic receptor activity at the base of outer hair cells *via* α9 nicotinic receptor knock-in reduced ABR fluctuations following low-intensity noise exposure (*45*). However, in our study, cholinergic nerve activation did not effectively rescue noise-induced auditory changes. This suggests the critical role of dopaminergic nerves in this process, while also indicating that cholinergic nerves cannot adequately compensate, as shown in our work, with the activated but disorganized cholinergic nerves.

Notably, the change in auditory sensitivity did not constitute conventional hearing loss, evidenced by significant alterations in ABR thresholds, DPOAE thresholds, or marked reductions in ribbon synapse numbers. Instead, it primarily manifested as alterations in cochlear efferent nerve fibers and amplified following mild to moderate noise exposure, as we have observed. However, this could not be described as the no differences in hearing and corresponding morphologic changes in mice. We interpret this phenomenon more as an early stage of hearing impairment based on the MPTP-induced PD mouse model. Research has demonstrated that functional hearing impairment is prevalent among PD patients, which precedes conventionally defined significant auditory changes (*37*). Some studies interpret hearing loss as a precursor to olfactory impairment (*3,46*). However, in our model, dopaminergic neurons in the substantia nigra are already significantly depleted. Therefore, interpreting the non-significant hearing impairment observed in our model as an early stage of PD-related hearing loss appears more appropriate, based on the MPTP-induced PD mice model.

Increasing clinical data have reported the lateralization of cochlear dysfunction in PD patients

(*5*). To elucidate the potential peripheral mechanisms underlying this phenomenon, we introduced 6-OHDA rat models with unilateral substantia nigra lesions. Notably, compared to bilateral 6-OHDA-induced rats, 6-OHDA-induced rats appear to be much more common in studies investigating the lateralization of PD (*46,47*). Furthermore, unilateral 6-OHDA injection yields higher postoperative survival rates (*48,49*), which is why we adopted this model. Furthermore, considering the potential risk of methamphetamine-induced hearing loss and the necessity of verifying successful model establishment through its-induced rotational movements (*23,24,50-52*), we adopted the more appropriate open-field test. Combined with the pathological feature of significant loss of dopaminergic neurons in the unilateral substantia nigra, this confirmed the successful establishment of the model.

Notably, compared to mouse PD models, where changes in ABR, DPOAE, hair cells, and synapses were insignificant, the PD rat model exhibited more pronounced alterations. Additionally, we also observed lateralization of peripheral auditory changes in the unilateral 6-OHDA-induced PD rat that hearing in the contralateral ear appeared worse than in the ipsilateral ear, followed by greater loss in hair cells and synapses of apical and basilar turns in the contralateral cochlea.

Previous studies have suggested that MOC and LOC may contribute to unilateral hearing loss in PD (*32*). Therefore, we labeled the LOC and MOC systems in rats. Interestingly, compared to PD mouse models, cholinergic neurons in the MOC showed no significant alterations, whereas those in the LOC exhibited bilateral asymmetric changes. A similar pattern of asymmetry was also observed in dopaminergic neurons. Unexpectedly, dopaminergic neurons displayed asymmetric activation rather than the pronounced structural and functional inhibition observed in mice, which may correlate with the 6-OHDA modeling approach (*26*). Increasing studies suggested that nigrostriatal dopaminergic neurons primarily innervate the auditory system through corresponding dopamine receptors or other types of nerve fibers (*10,15*), and the auditory system possesses an independent dopaminergic system separate from the nigrostriatal pathway (*53*). Following the death of substantia nigra dopaminergic neurons, the overall dopamine levels decrease, potentially leading to compensatory activation of dopaminergic neurons in the auditory system. However, due to the reciprocal innervation between the nigrostriatal and auditory systems, this compensation may be asymmetric (*32*). This compensation not limited to dopaminergic neuron, studies indicate complex connections also exist between cholinergic neurons and the auditory system (*54*). Furthermore, recent research suggests direct links may exist between basal ganglia regions, including the substantia nigra, and the auditory system (*15*). Consequently, unilateral nigral dopamine depletion may induce alterations in the central auditory system, which, together with ipsilateral compensatory changes in the LOC and MOC systems, could influence peripheral hearing thresholds and susceptibility. However, whether these LOC and MOC changes are secondary to nigral dopamine lesions or occur concurrently remains inconclusive. Additionally, we observed colocalization of cholinergic and dopaminergic elements within the LOC system showed bilateral asymmetric changes. Notably, although the sympathetic nerve located in the OSL did not show the marked depletion observed in mouse models, its reduction was still more pronounced on the surgical side, which aligns with our hypothesis that the central auditory system contributes to peripheral hearing pathology in PD models possibly.

Compared to the more extensive pathological damage observed in MPTP mouse models — including bilateral substantia nigra dopamine depletion, dopaminergic fibers loss in the cochlea, sympathetic fibers loss, and widespread cholinergic neuron activation, the 6-OHDA rat model — characterized by unilateral substantia nigra dopaminergic damage and bilateral asymmetric yet mild cholinergic and dopaminergic alterations — appears to correlate with more severe audiological and corresponding pathological changes. This discrepancy may be partly due to differences in molding methods and medications. Moreover, due to cross-innervation and functional complementarity between the central and peripheral nervous systems, unilateral substantia nigra dopamine depletion seems to elicit widespread compensatory mechanisms across both domains. Such compensatory responses are particularly common in neural lesion models (*55*).

5. Conclusion

In summary, we presented, for the first time, hearing alterations, pathological features, and potential mechanisms in the cochlea of MPTP-induced mouse and 6-OHDA-induced rat PD models, with particular focus on the role of efferent fibers. Furthermore, we, for the first time, reported denervation of adrenergic sympathetic fibers and ipsilateral peripheral hearing loss in MPTP-induced mouse and 6-OHDA-induced rat PD models, respectively. However, this study did not definitively explain whether loss of adrenergic sympathetic fibers in the MPTP model is a consequence of substantia nigra dopaminergic lesions. And due to the complexity of research involving both central auditory pathways and substantia nigra dopaminergic systems, we were unable to conduct more detailed investigations into central auditory changes and their secondary effects on peripheral hearing in the 6-OHDA-induced rat model. Furthermore, the pathogenesis of PD appears to be more complex, and currently, there is no PD animal model that can explain the total clinical progression in PD perfectly. Beyond the two classic models mentioned in our work,

additional models exist to simulate PD at different stages and under varying pathological conditions, which may also exhibit varying degrees of auditory changes but need further investigation. Thus, our findings were based only on studies using two classical animal models of PD and could not be fully equated with the clinical manifestations observed in PD patients. Moreover, most current clinical hearing studies in PD patients rely on tests like PTA, which can only evaluate significant hearing loss but not central auditory damage, hidden hearing loss, and functional hearing impairment. Further research should focus on these types of hearing impairment in clinical PD patients. In addition, age and other diseases causing cognitive impairment may confound hearing loss in PD patients (*56,57*). These factors limited our interpretation of many findings observed in this work.

Funding: This work was supported by the National Key Research and Development Program of China (2023YFC2508401, 2023YFC2508403, and 2023YFC2508405) and the Beijing Natural Science Foundation (7252145).

Conflict of Interest: The authors have no conflicts of interest to disclose.

References

1. Buonocore J, Iaccino N, Torchia G, Curcio F, Pirrotta FM, Contrada M, Pucci C, Gambardella A, Quattrone A, Pilotto A, Pignolo L, Arabia G. Cognitive stimulation in Parkinson's disease with mild cognitive impairment. J Neurol. 2025; 272:658.
2. Jafari Z, Kolb BE, Mohajerani MH. Auditory dysfunction in Parkinson's disease. Mov Disord. 2020; 35:537-550.
3. Simonet C, Bestwick J, Jitlal M, *et al*. Assessment of risk factors and early presentations of Parkinson disease in primary care in a diverse UK population. JAMA Neurol. 2022; 79:359-369.
4. Neilson LE, Reavis KM, Wiedrick J, Scott GD. Hearing loss, incident Parkinson disease, and treatment with hearing aids. JAMA Neurol. 2024; 81:1295-1303.
5. Lasheen RM, Elsheikh MN, Tomoum MO. Asymmetrical auditory dysfunction as a potential nonmotor lateralizing sign in Parkinson's disease: A case-control study. Otol Neurotol. 2025; 46:e370-e376.
6. Garasto E, Stefani A, Pierantozzi M, Cerroni R, Conti M, Maranesi S, Mercuri NB, Chiaravalloti A, Schillaci O, Viziano A, Moleti A, Sisto R. Association between hearing sensitivity and dopamine transporter availability in Parkinson's disease. Brain Commun. 2023; 5:fcad075.
7. Reijntjes DOJ, Pyott SJ. The afferent signaling complex: Regulation of type I spiral ganglion neuron responses in the auditory periphery. Hear Res. 2016; 336:1-16.
8. Hoyt JM, Perkel DJ, Portfors CV. Dopamine acts *via* D2-like receptors to modulate auditory responses in the inferior colliculus. eNeuro. 2019; 6:ENEURO.0350-19.2019.
9. Nevue AA, Elde CJ, Perkel DJ, Portfors CV. Dopaminergic input to the inferior colliculus in mice. Front Neuroanat. 2016; 9:168.
10. Maison SF, Liu XP, Eatock RA, Sibley DR, Grandy DK, Liberman MC. Dopaminergic signaling in the cochlea: Receptor expression patterns and deletion phenotypes. J Neurosci. 2012; 32:344-355.
11. Steenken F, Pektaş A, Köppl C. Age-related changes in olivocochlear efferent innervation in gerbils. Front Synaptic Neurosci. 2024; 16:1422330.
12. Lauer AM, Jimenez SV, Delano PH. Olivocochlear efferent effects on perception and behavior. Hear Res. 2022; 419:108207.
13. Darrow KN, Simons EJ, Dodds L, Liberman MC. Dopaminergic innervation of the mouse inner ear: Evidence for a separate cytochemical group of cochlear efferent fibers. J Comp Neurol. 2006; 498:403-414.
14. Barr HJ, Wall EM, Woolley SC. Dopamine in the songbird auditory cortex shapes auditory preference. Curr Biol. 2021; 31:4547-4559.e5.
15. Chen APF, Malgady JM, Chen L, Shi KW, Cheng E, Plotkin JL, Ge S, Xiong Q. Nigrostriatal dopamine pathway regulates auditory discrimination behavior. Nat Commun. 2022; 13:5942.
16. Hjelmervik H, Hausmann M, Bless JJ, Harkestad N, Hugdahl K, Laloyaux J. Estradiol driven change in hallucination proneness across the menstrual cycle as studied with a white noise paradigm. Psychoneuroendocrinology. 2024; 159:106410.
17. Jackson-Lewis V, Przedborski S. Protocol for the MPTP mouse model of Parkinson's disease. Nat Protoc. 2007; 2:141-151.
18. Wang Y, Chen R, Shi G, Huang X, Li K, Wang R, Cao X, Yang Z, Zhao N, Yan J. Chitosan alleviates symptoms of Parkinson's disease by reducing acetate levels, which decreases inflammation and promotes repair of the intestinal barrier and blood-brain barrier. Neural Regen Res. 2026; 21:377-391.
19. Yang B, Liu H, Zhang S, Liu B, Sun Q, Li W, Zheng R, Cui Q, Gu Y, Li X, Zhang J, Liu Y, Zhang F. Pharmacological and electrophysiological characterization of the novel Kv7 channel inhibitor racecadotril in Parkinson's disease. Neuropharmacology. 2025; 278:110565.
20. Wu Z, Dai J, Lv B, Su C, Xu D. Striatal metabolomic alterations in a mouse model of Parkinson's disease: A comprehensive liquid chromatography-mass spectrometry analysis. IBRO Neurosci Rep. 2025; 19:562-567.
21. Guo Q, Wang Y, Yu L, Guan L, Ji X, Li X, Pang G, Ren Z, Ye L, Cheng H. Nicotine restores olfactory function by activation of prok2R/Akt/FoxO3a axis in Parkinson's disease. J Transl Med. 2024; 22:350.
22. Kim W, Tripathi M, Kim C, *et al*. An optimized Nurr1 agonist provides disease-modifying effects in Parkinson's disease models. Nat Commun. 2023; 14:4283.
23. Basu S, Dudhabhate BB, Mitra S, Srivastava A, Pradhan P, Goswami C, Kokare DM, Singru PS. Transient receptor potential vanilloid 2 (TRPV2) channels modulate the nigrostriatal dopaminergic activity in rats. Neuropharmacology. 2025; 278:110545.
24. Liu K, Hui Y, Yang Y, Guo Y, Zhang L. Blockade of mGluR1 and mGluR5 in the lateral habenula produces the opposite effects in the regulation of depressive-like behaviors in the hemiparkinsonian rats. Exp Neurol. 2025; 386:115154.
25. Wu X, Hui Y, Wang L, Qiao H, Wang Y, Bai Y, Sun Q, Yang S, Yang J, Zhang Q, Li L. GluN2B in the dorsal hippocampus is involved in regulation of

hippocampus-dependent memory in Parkinsonian rats. Neuropharmacology. 2026; 282:110719.
26. Wu X, Hui Y, Wang L, Qiao H, Wang Y, Bai Y, Sun Q, Gao S, Zhang Q, Li L. Long-term intermittent theta burst stimulation alleviates Parkinson's disease-related cognitive impairment by modulating GluN2B in the dorsal hippocampus. Exp Neurol. 2025; 394:115439.
27. Wu JS, Yi E, Manca M, Javaid H, Lauer AM, Glowatzki E. Sound exposure dynamically induces dopamine synthesis in cholinergic LOC efferents for feedback to auditory nerve fibers. Elife. 2020; 9:e52419.
28. Wu JS, Vyas P, Glowatzki E, Fuchs PA. Opposing expression gradients of calcitonin-related polypeptide alpha (Calca/Cgrpα) and tyrosine hydroxylase (Th) in type II afferent neurons of the mouse cochlea. J Comp Neurol. 2018; 526:425-438.
29. Wang W, Yu L, Li S, Han L, Zheng H. NFAT3-FasL axis synchronously regulates apoptosis and necroptosis in murine cochlear outer hair cells after noise trauma. Front Mol Neurosci. 2024; 17:1422646.
30. Athari SZ, Farajdokht F, Karimipour M, Alipour MR, Mohaddes G. Intranasal AdipoRon improves motor function in a rat model of Parkinson's disease by promoting neurogenesis in the nigrostriatal pathway. Neuropharmacology. 2025; 281:110687.
31. Atamna Y, Tiroshi L, Wattad N, Gilin N, Gilad S, Berkowitz N, Goldberg JA. Levodopa disrupts activity patterns and encoding of movement in striatal cholinergic interneurons of behaving mice. Mov Disord. 2025; 40:2457-2468.
32. Sisto R, Viziano A, Stefani A, Moleti A, Cerroni R, Liguori C, Garasto E, Pierantozzi M. Lateralization of cochlear dysfunction as a specific biomarker of Parkinson's disease. Brain Commun. 2020; 2:fcaa144.
33. Rimal N, Khanal S, Bohara G, Choi DY. Exendin-4 protects the dopaminergic neurons by attenuating inflammatory responses of microglial cells *via* activation of AMPK. Neuropharmacology. 2025; 279:110643.
34. Wu WJ, Lu CW, Wang SE, Lin CL, Su LY, Wu CH. MPTP toxicity causes vocal, auditory, orientation and movement defects in the echolocation bat. Neuroreport. 2021; 32:125-134.
35. Le Prell CG, Halsey K, Hughes LF, Dolan DF, Bledsoe SC Jr. Disruption of lateral olivocochlear neurons *via* a dopaminergic neurotoxin depresses sound-evoked auditory nerve activity. J Assoc Res Otolaryngol. 2005; 6:48-62.
36. Wang H, Aiken SJ, Wang J. Consequences and mechanisms of noise-induced cochlear synaptopathy and hidden hearing loss, with focuses on signal perception in noise and temporal processing. Adv Sci (Weinh). 2025; 12:e2409322.
37. Jose M, Nene D, Choi MWY, Yu AC, Small J, Mirian M, Jenstad L, Appel-Cresswell S. Functional hearing impairment common in Parkinson's disease: Insights from a pilot study. Clin Neurol Neurosurg. 2024; 246:108524.
38. Dörje NM, Shvachiy L, Kück F, Outeiro TF, Strenzke N, Beutner D, Setz C. Age-related alterations in efferent medial olivocochlear-outer hair cell and primary auditory ribbon synapses in CBA/J mice. Front Cell Neurosci. 2024; 18:1412450.
39. Carmona-Abellan M, Martínez-Valbuena I, DiCaudo C, Marcilla I, Luquin MR. Cardiac sympathetic innervation in the MPTP non-human primate model of Parkinson disease. Clin Auton Res. 2019; 29:415-425.
40. Masilamoni GJ, Weinkle A, Papa SM, Smith Y. Cortical serotonergic and catecholaminergic denervation in MPTP-treated Parkinsonian monkeys. Cereb Cortex. 2022; 32:1804-1822.
41. Oizumi H, Yamasaki K, Suzuki H, Ohshiro S, Saito Y, Murayama S, Sugimura Y, Hasegawa T, Fukunaga K, Takeda A. Phosphorylated alpha-synuclein in Iba1-positive macrophages in the skin of patients with Parkinson's disease. Ann Clin Transl Neurol. 2022; 9:1136-1146.
42. Isonaka R, Goldstein DS, Zhu W, Yoon E, Ehrlich D, Schindler AB, Kokkinis AD, Sabir MS, Scholz SW, Bandres-Ciga S, Blauwendraat C, Gonzalez-Alegre P, Lopez G, Sidransky E, Narendra DP. α-Synuclein deposition in sympathetic nerve fibers in genetic forms of parkinson's disease. Mov Disord. 2021; 36:2346-2357.
43. Tian C, Zha D. Sympathetic nervous system regulation of auditory function. Audiol Neurootol. 2022; 27:93-103.
44. Liang C, Zhai TY, Chen J, Fang S, Zhu Y, Liu LM, Yu N, Zhao HB. ATP-gated P2x7 receptors express at type II auditory nerves and are required for efferent hearing control and noise protection. Proc Natl Acad Sci U S A. 2025; 122:e2421995122.
45. Boero LE, Castagna VC, Di Guilmi MN, Goutman JD, Elgoyhen AB, Gómez-Casati ME. Enhancement of the medial olivocochlear system prevents hidden hearing loss. J Neurosci. 2018; 38:7440-7451.
46. Cunha AM, Teixeira FG, Guimarães MR, Esteves M, Pereira-Mendes J, Soares AR, Almeida A, Sousa N, Salgado AJ, Leite-Almeida H. Unilateral accumbal dopamine depletion affects decision-making in a side-specific manner. Exp Neurol. 2020; 327:113221.
47. Nascimento GC, Jacob G, Milan BA, Leal-Luiz G, Malzone BL, Vivanco-Estela AN, Escobar-Espinal D, Dias FJ, Del-Bel E. Brainstem modulates Parkinsonism-induced orofacial sensorimotor dysfunctions. Int J Mol Sci. 2023; 24:12270.
48. Rajneesh CP, Hsieh TH, Chen HC, Liou JC, Lin BS, George Wu CW, Lai CH, Peng CW. A time-course study of urodynamic analyses in rat models with dopaminergic depletion induced through unilateral and bilateral 6-hydroxydopamine injections. J Formos Med Assoc. 2023; 122:239-248.
49. Ungerstedt U. Adipsia and aphagia after 6-hydroxydopamine induced degeneration of the nigro-striatal dopamine system. Acta Physiol Scand Suppl. 1971; 367:95-122.
50. Reich JS, Sethi HK, Sataloff RT. Bilateral sensorineural hearing loss in the setting of acute methamphetamine overdose. Ear Nose Throat J. 2024; 103:NP491-NP493.
51. Charles KA, Molpeceres Sierra E, Bouali-Benazzouz R, Tibar H, Oudaha K, Naudet F, Duveau A, Fossat P, Benazzouz A. Interplay between subthalamic nucleus and spinal cord controls parkinsonian nociceptive disorders. Brain. 2025; 148:313-330.
52. Cheng Y, Wang G, Yang X, Wang Y, Li D, Zhao Y, Zhang F. Artesunate alleviates Parkinson's disease by targeting astrocyte MT2A to attenuate dopamine neuronal cuproptosis. Pharmacol Res. 2025; 219:107895.
53. Harris S, Afram R, Shimano T, Fyk-Kolodziej B, Walker PD, Braun RD, Holt AG. Dopamine in auditory nuclei and lemniscal projections is poised to influence acoustic integration in the inferior colliculus. Front Neural Circuits. 2021; 15:624563.
54. Bohnen NI, Yarnall AJ, Weil RS, Moro E, Moehle MS, Borghammer P, Bedard MA, Albin RL. Cholinergic

system changes in Parkinson's disease: Emerging therapeutic approaches. Lancet Neurol. 2022; 21:381-392.
55. Rairan LG, Henriquez A, Diaz G, Mejía JA, Gomez D, Ramon JF, Hakim EJ. Unveiling the current understanding of idiopathic spinal cord herniation: A systematic review. Spine Surg Relat Res. 2023; 8:225-234.
56. Asakawa T, Yang Y, Xiao Z, Shi Y, Qin W, Hong Z, Ding D. Stumbling blocks in the investigation of the relationship between age-related hearing loss and cognitive impairment. Perspect Psychol Sci. 2024; 19:137-150.
57. Peng Y, Song P, Karako T, Asakawa T. Blocking progression from intervenable mild cognitive impairment to irreversible dementia, what can we do? Biosci Trends. 2024; 18:409-412.

Received October 27, 2025; Revised December 1, 2025; Accepted December 18, 2025.

[§]These authors contributed equally to this work.
**Address correspondence to:*
Lisheng Yu, Yixu Wang, and Hongwei Zheng, Department of Otorhinolaryngology, Head and Neck Surgery, Peking University People's Hospital, No.11 Xizhimen South Street, Xicheng District, Beijing 100044, China.
E-mail: yulish68@163.com (LY), yixu2007@163.com (YW), and zhenghongwei@pku.edu.cn (HZ)

Released online in J-STAGE as advance publication December 20, 2025.